Biomass and Bioenergy 177 (2023) 106930

Contents lists available at ScienceDirect

Biomass and Bioenergy

journal homepage: www.elsevier.com/locate/biombioe

Biochar and other carbonaceous materials used in steelmaking: Possibilities and synergies for power generation by direct carbon fuel cell

Gianluca Dall'Osto *, Davide Mombelli, Andrea Pittalis, Carlo Mapelli

Politecnico di Milano, Dipartimento di Meccanica, Via La Masa 1, 20156, Milano, Italy

ARTICLE INFO

Keywords:
Biochar
Direct carbon fuel cell
Carbonaceous materials
Steelmaking
Emission reduction

ABSTRACT

The objective of this study is the preliminary investigation of the feasibility of using a low-temperature molten hydroxide direct carbon fuel cell as an additional energy source for steel production by electric arc furnace. For this purpose, four carbonaceous materials related to the steel industry (electrographite, coke, torrefied biochar and hydrochar) were selected and characterized to predict their electrical behavior before their actual introduction as fuels. Special attention was paid to both the morphological effect (bulk/pellet or powder) and the chemical composition of the fuels on the electrical performance of the cell. Electrical measurements showed the positive influence of powder morphology, with coke powder having the highest peak power density value (49.6 mW/cm^2). Electrographite was found to be useable only as a powder (18.7 mW/cm^2), as the high chemical stability of the bulk morphology, provided by the smooth surface and the pitch used as a binder, acted as inhibitors of the carbon oxidation reaction. Although biochar appeared superior to hydrochar when inserted as powder (23.5 vs. 18.2 mW/cm^2), the latter showed promising results also inserted as pellet. the latter also showed promising results when inserted as a pellet. Specifically, once inserted within the molten hydrochar, the binder used to produce the hydrochar is removed changing the morphology from pellet to sandy/powdery, negating the penalizing effect of the lower surface to volume of bulk morphology (15.8 vs. 18.2 mW/cm^2) and offering the advantage of avoiding the milling process and related fine particulate production from an industrial point of view.

1. Introduction

Despite its vital importance in several industrial sectors, steelmaking is actually considered as an hard-to-abate industry, being responsible for 7% of the world total CO_2 emission and about 8% of global energy demand [1–3]. Replacement of fossil carbon feedstocks, substantial modifications and upgrades of existing processes and the introduction of Carbon Capture and Storage (CCS) technologies into current production processes are the three most discussed pathways for the emissions mitigation [4–8]. In addition to these, steel production through scrap recycling and melting inside the electric arc furnace (EAF) is expected to steadily increase in the coming decades, at the expense of the currently more widespread integrated cycle based on hot metal production from iron ore inside the blast furnace (BF), mainly due to the lower direct CO_2 emission of the former (10^2 kg_{CO2}/t_{STEEL} vs. 10^3 kg_{CO2}/t_{STEEL}) [6,9,10]. Furthermore, several efforts and studies have been conducted over the past decade, both on a laboratory and industrial scale, to investigate the actual feasibility of biomass derived carbonaceous material as a substitute for fossil carbon sources, Table 1 reports some of the possibilities investigated, focusing on biochar and hydrochar as material used.

However, to fully understand the sustainability of the scrap recycling route, it is also necessary to consider the specific electrical requirements, which are currently five times higher than those of the integrated cycle, thus representing the most burdensome indirect emission factor [6]. As a matter of fact, countries still relying on coal-fired power generation would benefit from only a slight decrease in overall emissions (e.g., 14.7% at most in the Australian scenario) even in the case of a complete substitution of fossil carbon sources with biomass as reductants in the EAF [4,22,23]. At the same time, if the same scenario is applied to the EU-27, the potential reduction in emissions would rise to 29% due to the increase in the share of electricity generation from renewable sources, which is about 27% in 2019 and 37% if also nuclear energy is accounted [24,25].

Taking inspiration from the energy and cement sectors, the application of Molten Carbonate Fuel Cells (MCFCs) as an additional energy

* Corresponding author.
E-mail address: gianluca.dallosto@polimi.it (G. Dall'Osto).

https://doi.org/10.1016/j.biombioe.2023.106930
Received 24 October 2022; Received in revised form 7 July 2023; Accepted 27 August 2023
Available online 6 September 2023

Table 1
Examples of biochar and hydrochar main usages in the steel production cycle.

Main usage	Carbonaceous materials used and sources
Coal substitution	Biochar [11–14], Hydrochar [11,12]
Carburizing agent in EAF	Biochar [15,16], Hydrochar [16]
Foaming agent in EAF	Biochar [17], Hydrochar [16]
Injection in blast furnace	Biochar [18], Hydrochar [18–21]

source is also highly appealing for the steelmaking sector, since it would help to mitigate indirect emissions [26–29]. However, since MCFCs are able to act as CO_2 concentrating and capturing devices while still generating additional power, their application would be more effective and appropriate for the integrated cycle than for an electric mill due to the higher amount of emissions of the former [26–29].

Therefore, it is necessary to understand which of the various types of fuel cells is the most synergistic in the context of scrap recycling. Considering the fuel type and temperature requirements, Direct Carbon Fuel Cells (DCFCs) appear to be one of the most promising candidates. These type of fuel cells are based on the direct conversion of chemical energy contained in carbon, which is introduced as a solid fuel, into electricity without the need for gasification (overall reactions highlighted in Eqs. (1) and (2)) at an operating temperature in the range of 600–900 °C [30,31].

$$O_2(air) + 4e^- = 2O^{2-} \quad (1)$$

$$C + 2O^{2-} = CO_2 + 4e^- \quad (2)$$

Moreover, because fuel theoretical utilization is close to unity and, unlike other types of fuel cells, the theoretical thermodynamic efficiency is independent of temperature, it is possible to work at lower temperature, than 600 °C if appropriate electrolytes are used (e.g., molten hydroxides), without any significant disadvantage [30,32,33]. Finally, considering the system-based losses, a theoretical stack efficiency of 0.8–0.85 or even higher is expected, which is almost twice as much as a conventional coal-fired plant, with the main advantage of a pure CO_2 outflow which can be easily captured by CCS for downstream use or disposal, avoiding the need for additional costly gas separation and purification technologies [30,34].

Since two of the parameters governing cell performance are fuel quality (*C content/inorganic matter*) and surface-to-volume ratio (*S/V*), most of the carbon bearing materials already in the scrap recycling cycle are more than suitable without the need for specific pretreatment.

A first case would be the valorization of electrographite furnace electrodes, which have broken during installation or service life (e.g., due to improper material charging or arc length) as they are characterized by low electrical resistance, high graphitization and consequently purity. However, the use of this carbon source is highly dependent on its economic value, which can be subject to several fluctuations, as in recent years [35].

Therefore, the benefits of its introduction as an energy source within a DCFC should be weighed against the amount of energy and emission savings that can be achieved, especially compared to other candidate carbon materials (e.g., coke, coal, and biomass) already present in the steel industry. At present, coke and anthracite coal are mainly used in EAFs for the slag foaming practice and inserted in the process as powder by means of pneumatic injection [4]. On the other hand, since the process is highly dependent on both the technological parameters and the physical properties of the powders themselves, the introduction of carbonaceous materials with high volatile matter, such as biomass or plastic wastes, is limited unless specific pretreatment or blending with coke is carried out [36–38]. Consequently, it is difficult to determine a specific lower threshold of particle size that will lead to operational problems for the steel production. However, considering the values used for numerical simulations of the process in the literature, it is possible to define indicative diameters ranging from hundreds of μm to mm, depending mainly on the type of carbon source introduced [36–40].

Indeed, in the case of incorrect parameters or too low particle size, some of the injected powder may leak into the upper region of the EAF and be sucked out of the fourth hole, then collected in bag filters placed in the off-gas treatment section, or consumed in post-combustion, and thus leading to a worse utilization of the available carbon in the furnace and consequently an increase in production costs and wasted feedstock [41,42]. Finally, in the worst-case scenario, these powders could also be dispersed into the mill environment or nearby areas, enhancing the risk of occurrence of human health diseases related to poor air quality [43–45]. In contrast, the introduction of powders, with a granulometry higher than hundreds of μm, as fuels for DCFCs could easily avoid these issues and improve cell performance by exploiting their high S/V ratio. In addition, the carbon footprint would be discounted if the carbonaceous materials were originated from biogenic sources, as in the case of biomass [46–50]. It is interesting to note that, in Italy alone, the production of organic waste has had an average annual increase of 5.6% over the past decade, reaching a total value of 7.2 Mton in 2021, of which approximately two thirds is disposed in landfills or burned [51]. On the other hand, it would be possible to valorize them through appropriate carbonization processes which would allow their introduction not only into the steelmaking processes, as substitutes for fossil carbon, but also as fuels in a DCFC. Therefore, assuming to carry out on the wet fraction a hydrothermal carbonization process and a slow pyrolysis process on the solid part, with a conservative yield of 0.4 and 0.3, respectively, it would be possible to achieve a potential production of 1.96 Mton of hydrochar and 0.7 Mton of biochar [52–54].

Finally, even though steelmaking processes operate at some of the highest temperatures among all industrial processes, only a small portion of the associated waste heat available (e.g., charge melting, slag cooling, flue gases) is exploited at industrial scale [55–58]. Indeed, as stated by Zhang et al. [59], the current waste heat recovery rate of the steel industry is only at 17%, whereas in China the value reaches 26% according to Yue et al. [60]. Consequently, several studies and industrial trials have tried to exploit this energy source, focusing mainly (i.e., by means of organic Rankine cycle systems) [61,62]. Furthermore, Salimbeni et al. [63] investigated the feasibility of using the thermal energy available in EAF flue gas on a pilot plant scale to heat a slow pyrolysis furnace operating at a temperature of 550 °C to produce wood charcoal, as a substitute for coal, further emphasizing the key current and future role that biochar and alternative waste-to-power technologies will play in the steel industry. Consequently, given the wide availability of such energy sources, it is more than reasonable to exploit them to provide the total or partial heat needed to melt the fuel cell electrolyte, further increasing the efficiency of the process and possible power generation.

In particular, using an eutectic mixture of hydroxides (e.g., NaOH and KOH), it would be possible to operate at relatively low temperature (450–700 °C) while maintaining acceptable ionic conductivity [32,64].

In this work, four carbonaceous materials related to the steel industry were used as fuels for a MH-DCFC to assess the feasibility of its use as an additional energy source for the steel production by EAF, thereby reducing the indirect emissions associated with the use of fossil carbon based energy sources. Each material was first characterized through thermal and mineralogical analyses. On one hand, electrical analyses focused on comparing the performance achieved by each fuel, and on the other hand, on the influence of fuel morphology (bulk/pelletized and powdered) and chemical composition.

2. Material and methods

2.1. Materials

The carbonaceous materials used as fuels were chosen by taking into account their current or future presence in steelmaking processes: 1) electrographite (GR) obtained from the residue of an EAF electrode broken during installation, 2) coke (CO), which is the feedstock with the

greatest environmental impact used in the steelmaking processes, 3) pelletized biochar (BC) obtained from the torrefaction process of wood chips and 4) pelletized hydrochar (HC) produced by hydrothermal carbonization of sewage sludge.

2.2. Materials characterization

Thermogravimetric and Differential Scanning Calorimeter (TG-DSC) was used to perform the proximate analysis characterization on the four carbonaceous materials, based on a modified version of the ASTM D1762-84 standard [65]. Approximately 10 mg of each sample was subjected to heating from room temperature to 1000 °C under nitrogen gas flow (heating rate: 10 °C/min), held for 10 min and then cooled from 1000 to 300 °C (cooling rate: 10 °C/min) to quantify the amount of moisture (M) and volatile matter (VM). Then, the atmosphere was switched to air and the sample was subjected to a second heating to 1000 °C (heating rate: 10 °C/min) to allow the oxidation reaction to take place, the remaining mass residue was considered as ash (A). The percentage of fixed carbon (FC) was determined by the following mass balance:

$$FC = 100 - (M + VM + A)$$

The mineralogical evolution during heating and operation in the fuel cell and the chemical composition of the fuels ash was evaluated by heating each material in an oxidizing environment using a muffle furnace at four different temperatures (105, 450 and 750 °C, heating rate 50 °C/min and 1 h holding time). Phase determination was carried out by X-Ray Diffraction (XRD) (scattering angle from 5° to 80°, step of 0.02°, scan speed 1°/min at 40 kV, 40 mA using Cu-Kα radiations) after samples pulverization below 100 μm to decrease the effect of the material texture. The crystallinity degree was calculated for each sample as the ratio of the area of the crystalline phases peaks to that of the total XRD spectrum.

2.3. MH-DCFC cell design

A laboratory-scale Molten Hydroxide DCFC (MH-DCFC) cell was developed to carry out the electrical analysis on each sample (Fig. 1). To ensure sufficient corrosion resistance over time against the hydroxide mixture, the crucible, which served as the electrolyte container and cathode, was made of INCONEL 625 (inner diameter: 85 mm, height: 135 mm) [66,67].

The fuel was enclosed in an AISI 304 mesh properly folded to achieve a geometry similar to that of a tea bag (total exchange area: 2 mm^2), which served as the anode, and inserted through the crucible lid by means of an AISI 316L wire. As well as the crucible material selection, the choice to use a stainless steel was based on its corrosion resistance in an alkaline environment [68,69].

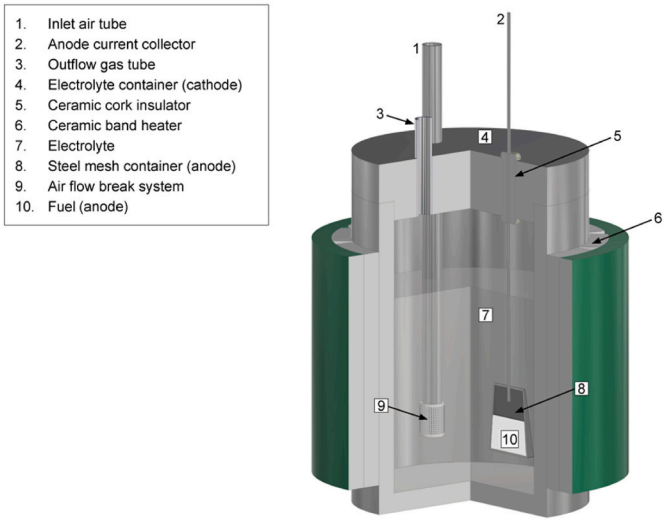

Fig. 1. Molten hydroxide direct carbon fuel cell design.

Finally, to insufflate the air required for the carbon oxidation, a straight tube made of INCONEL 625 (inner diameter: 8 mm) was used and inserted directly through the crucible lid; an airflow breaker system was inserted at the end of the tube to promote a proper air distribution within the electrolyte. The anode and cathode were electrically insulated through a ceramic cork.

The fuel cell was heated by a ceramic band heater and thermally insulated by ceramic wool; for safety and handling reasons, the whole system was placed inside a steel container and the two systems were electrically insulated. The electrolyte applied was a eutectic mixture of NaOH and KOH, as it has been observed to provide superior performance compared with other hydroxide mixtures (e.g., NaOH-LiOH and NaOH-KOH-LiOH), especially when biochar is used as a fuel, and to reduce it as much as possible (450 °C) [70]. Prior to the anode immersion into the molten electrolyte, air was blown into the molten electrolyte at a rate of 0.10 NL/min for 1 h to saturate the environment with oxygen, and then increased at 0.25 NL/min during the electrical measurements.

2.4. Electrochemical measurements

Electrical analyses were conducted on the four carbonaceous materials in two different morphologies: bulk granule/pelletized (C) and powder (P), the latter obtained after grinding to a granulometry ranging from 0.125 to 0.5 mm. Specifically, since sample G was too large to fit inside the laboratory DCFC, in the bulk morphology, its size was reduced to obtain a lump of prismatic geometry, while the remaining three samples were placed inside the steel mesh container in the condition as received (samples BC and HC as pellets, sample CO as a small lump). In contrast, the fuel in the powder morphology did not show any problems concerning its insertion inside the steel mesh container or the dispersion of the fine powders during the handling of the anode itself, due to the smaller opening of the mesh sieves with respect to the selected particle size.

To evaluate the influence of materials on fuel cell performance, Open Cell Voltage (OCV), Linear Scan Voltammetry (LSV) and galvanostatic analyses were performed by means of an AMEL potentiostat/galvanostat mod.2553 operated with Vpeak 2018 proprietary software. A two-electrode configuration was used for all electrical measurements.

The crucible served as working electrode (WE) and the fuel, placed inside the tea bag container, as counter electrode (CE). The OCVs were monitored for 90 min at the operating temperature of 450 °C prior to each test. Polarization began from the OCV value down to 10% of it with a potential scan rate of 0.5 mV/s at 450 °C. Two galvanostatic measurements were made by imposing firstly a current value equal to that corresponding to the maximum power density for 5 min and then at an imposed current equal to 100 mA.

Finally, to understand whether there was any modification of the steel mesh used as the fuel container during cell operation, which could lead to improper contact between the fuel, air, and electrolyte due to the generation of corrosion products that could close the mesh openings, it was characterized morphologically and chemically by SEM and XRD analysis at the end of each test.

3. Results and discussion

3.1. Materials characterization

The thermogravimetric and proximate analyses of the four materials are given in Table 2 and Fig. 2. TG-DSC analysis showed similar behaviors of the GR and CO samples, which were characterized by high stability and negligible mass loss in the first phase of heating (inert

Table 2
Proximate analysis of the materials used as fuel (GR: electrographite, CO: coke, BC: biochar, HC: hydrochar).

	Moisture [% wt.]	Volatile Matter [% wt.]	Fixed Carbon [% wt.]	Ash [% wt.]
GR	0.05	6.25	89.30	4.40
CO	1.00	5.20	85.20	8.60
BC	5.60	38.80	49.30	6.30
HC	4.50	66.80	0.66	28.04

environment), reflected in low moisture and volatiles (Table 1). In contrast, the BC and HC samples underwent significant mass reduction during the inert atmosphere stage, associated with the loss of volatile matter, with the HC sample consisting of more than 60% of it. It is possible to attribute the high amount of volatiles in the samples to the low pyrolysis temperature used in both the torrefaction and hydrothermal carbonization processes, since the amount of volatiles is highly dependent on the starting material, pyrolysis process and operating conditions (temperature, heating rate, residence time) [34,71].

The role and effect of volatile matter on the electrical performance of a DCFC is still debated in the literature. As a rule of thumb, it can be assumed that most of the volatile matter is composed of oxygen functional groups (e.g., -CO, -OH groups) or hydrocarbons, which contribute positively to the electrochemical processes that occur during cell operation, as they lower the overall resistance and improve electron flow [72,73].

In addition, a high amount of volatile matter can be advantageous for reaction kinetics, as on the one hand, it increases structure disorder (directly related to material reactivity), and on the other hand, it creates new surfaces within the bulk of the material (leading to a higher S/V ratio and gas diffusion) [74,75]. However, it has also been experienced that excessive volatiles can lead to the opposite effect on cell performance by hindering proper fuel oxidation [76]. This behavior could be due to the chemical nature of the volatile compounds, which depends on that of the starting pyrolyzed biomass, as it is possible that some of the elements in them could poison the cell materials, particularly the anode if constructed of Ni or Cu, hindering the overall electrical performance [34]. Therefore, it is necessary to chemically characterize each carbonaceous material in depth to understand its suitability as a fuel.

During the second heating ramp performed in air, each sample showed the typical peak associated with carbon combustion (Fig. 2). From the evaluation of its extent and the corresponding mass loss, it is possible to assess the amount of fixed carbon and to evaluate the ease of oxidation of the material, which is essential for the proper functioning of the cell.

In general, combustion occurred in the 500–760 °C temperature range, with the GR sample having the highest mass loss, followed by CO, BC, and HC, respectively (Table 2). On the other hand, the CO and BC samples initiate the combustion reaction at 460 °C, with the latter being characterized by peak splitting, higher combustion energy and associated mass loss, which could be advantageous for its application in a DCFC, as the higher reactivity implies a higher electrochemical reaction rate [77–79]. Finally, the combustion peak and mass loss of the HC sample appear negligible as a result of the high amount of volatile matter. In contrast, the HC sample was characterized by the highest amount of ash (28 %wt.), while the amount of ash in the remaining three samples fell within a range of 4 %wt. to 9 %wt. (Table 2).

Similar to volatile matter, total carbon and ash can affect cell performance. In particular, it is readily apparent that a high amount of carbon is necessary to achieve desirable efficiencies, however, too high percentages (>90% %wt.) can hinder light gas generation, lowering the kinetics of electrochemical reactions [49,77].

Instead, although a high amount of ash is not suggested, the compounds in them can act as both inhibitors and catalysts for the electrochemical oxidation of carbon, and therefore their presence and percentage must be evaluated on a case-by-case basis (e.g., SiO2 and Al2O3 are considered inhibitors, whereas K2O, CaO, MgO and Fe2O3 catalyzers) [49,80,81].

The evolution of mineralogical composition and crystallinity of fuels after heating in an oxidizing environment was studied by XRD analysis (Fig. 3).

The GR sample (Fig. 3a) showed no change after heating and a degree of crystallinity always 100%, with only one peak present associated with graphite (C, 26°). In addition to the graphite peak, the CO spectra (Fig. 3b) were characterized by the presence of quartz (SiO_2, 20.85° and 26.62°) and alumina (Al_2O_3, 12.50° and 34.55°), which can act as inhibitors during the cell operation due to the formation of an insulating

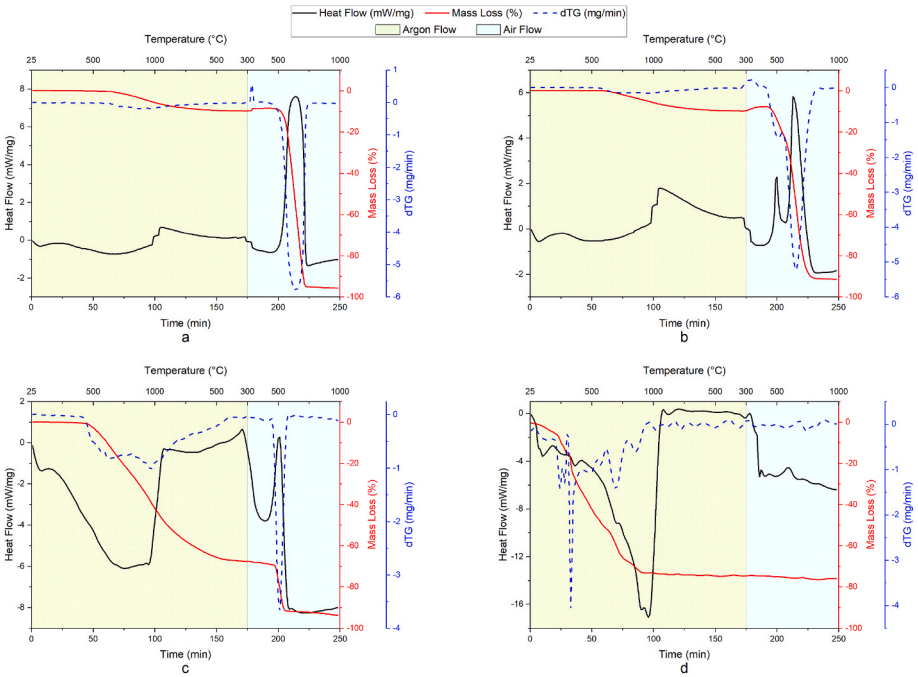

Fig. 2. TG-DSC curves used for the proximate analysis evaluation of the materials used as fuel (a) electrographite, (b) coke, (c) biochar and (d) hydrochar.

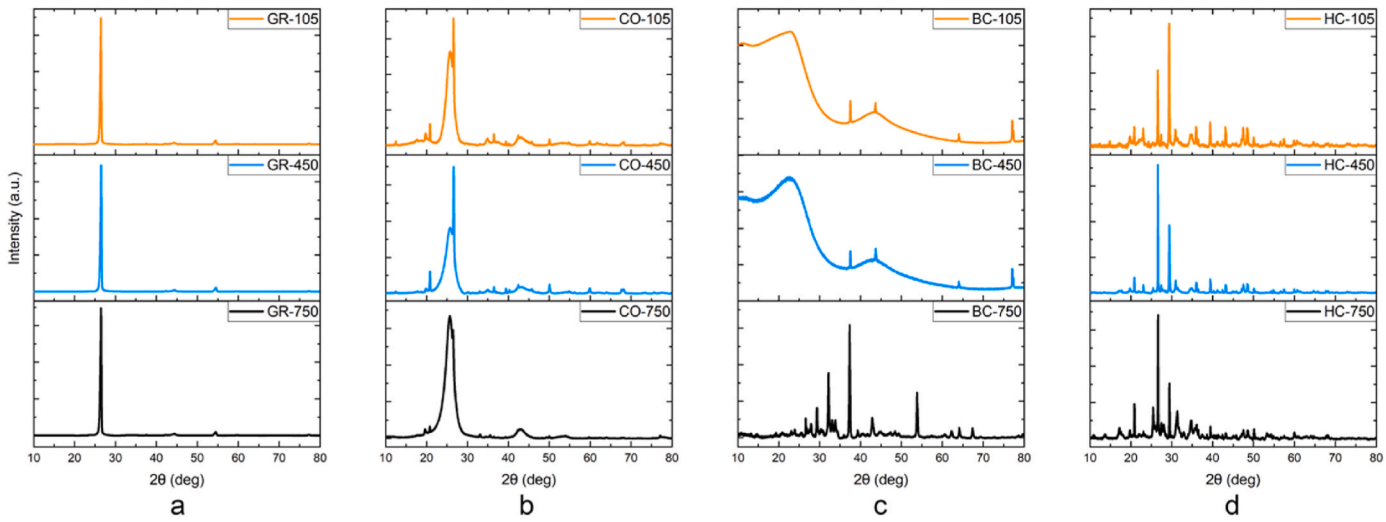

Fig. 3. XRD spectra of the materials used as fuel (a) GR: electrographite, (b) CO: coke, (c) BC: biochar and (d) HC: hydrochar.

film on the surface of the fuel that prevents its oxidation, while the remaining low intensity peaks were associated with the presence of illite ($Al_4KO_{12}Si_2$, 19.67°) [34,49]. The degree of crystallinity increased slightly from 80% to 88% (Fig. 3b CO-105 vs. CO-750) due to the removal of small impurities present as amorphous phases.

The BC spectra (Fig. 3c) changed their appearance after each heating, with a significant amount of amorphous carbon evidenced by the broad peak ranging from 15° to 30° in both BC-105 and BC-450 samples, and with only one crystalline phase associated with periclase (MgO, 37.88°, 44.02° and 64.01°). In addition, lime (CaO), calcite, quartz, and hematite (Fe_2O_3) were the main phases observed after carbon combustion (BC-750). Consequently, it can be said that the chemical composition of BC ash seems optimal for its introduction as a fuel in DCFC. Indeed, during the fuel cell operation, on the one hand, hematite should act as a catalyst and, on the other hand, lime could reduce capture part of the emitted CO_2 as a consequence of its carbonation reaction (Eq. (3)). Finally, the degree of crystallinity increased abruptly from almost zero to 77% at 750 °C.

$$CaO + CO_2 = CaCO_3 \quad (3)$$

Due to the lower temperature of the hydrothermal carbonization compared to the torrefaction process, the HC-105 spectrum (Fig. 3d) highlighted the presence of small residues of cellulose compounds, which completely disappear at the higher temperature due to exhaustion of their decomposition. The remaining main compounds observed in the HC-105 spectrum were quartz, calcite ($CaCO_3$), illite, wuestite (FeO), dolomite ($(Ca,Mg)CO_3$) and hydroxyapatite ($Ca_5(PO_4)_3OH$), the latter present in low percentages. Upon heating, the main identified phases remained stable, with just some modification of the peak intensities (Fig. 3d HC-105 vs. HC-450), whereas at to 750 °C, the oxidation of wuestite to hematite was observed together with the partial decomposition of dolomite into periclase and lime (Fig. 3d HC-450 vs. HC-750) [82–84].

Spectral analysis showed that a higher degree of crystallinity was obtained than in the BC sample, with an initial crystallinity of 70%, increasing to 90% at 750 °C.

According to the Rietveld analysis performed on the HC-750 spectrum, the HC ashes were composed for about 22 %wt. of the catalytic phases versus 7.2 %wt. of the inhibiting phases, which could positively influence the electrical performance during cell operation, despite the lower value of fixed carbon compared with the BC sample.

3.2. DCFC electrical performance

3.2.1. Open cell voltage

The OCV behavior was monitored continuously for 90 min, the CO powder sample is shown in Fig. 4 for discussion of typical OCV evolution.

Each fuel provided a similar trend, describable as inverse logarithmic, with an increase in the starting voltage as soon as the anode is inserted into the molten electrolyte due to the oxygen already present in it. Once the oxygen flux is increased from 0.10 to 0.25 NL/min, a small peak is observed, consistent with the expected effect of rising oxygen concentration from the Nernst equations [32].

Finally, after the increase in oxygen flow, the OCV continues to increase with some small fluctuation, probably due to increased turbulence within the electrolyte, until it reaches a stable value after about 90 min due to the stabilization of both temperature and oxygen partial pressure. The stabilized values after an additional 30 min are shown in Table 3.

The values obtained are consistent with those expected from other works utilizing different type of DCFCs, working temperatures, or materials, and in general all powder samples showed higher OCVs than

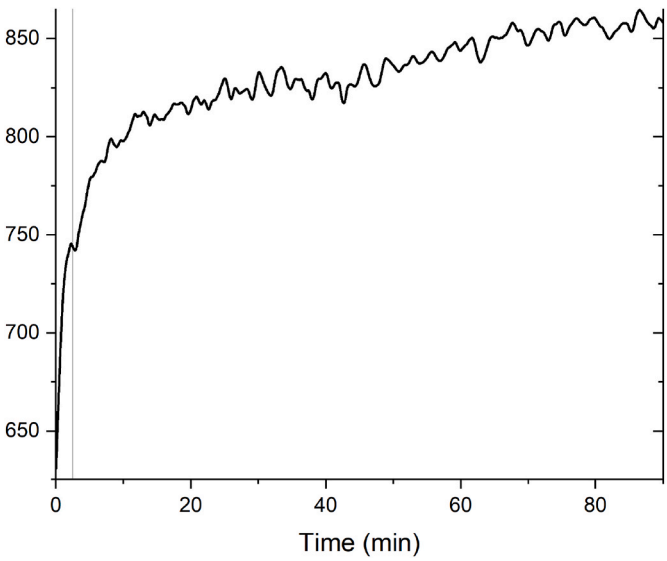

Fig. 4. Typical open cell voltage curve observed (straight vertical: change from 10 NL/min to 25 NL/min of oxygen flow).

Table 3
Open cell voltage values of the fuels (GR: electrographite, CO: coke, BC: biochar, HC: hydrochar, C: bulk/pelletized morphology, P: powder morphology).

	GR		CO		BC		HC	
	C	P	C	P	C	P	C	P
OCV [mV]	*260*	*705*	*780*	*880*	*475*	*850*	*950*	*980*

bulk samples due to higher S/V, especially the OCV of the GR-P sample is almost three times higher than that of GR-C [32,50,70,85–88].

The lower value obtained from the bulk sample may be due to the high chemical stability and smoothness of the electrographite surface. In addition, an important role could be due to the presence of complex mixture of aromatic or heterocyclic hydrocarbons contained in pitch, which is used as a binder in the production of electrodes for the electric arc furnace [89]. The presence of heteroatoms is more conducive to improving the capacitive property of the material than the electrical conductivity [90].

Sample BC also benefited from the higher S/V ratio provided by the powder morphology, increasing its OCV from 475 mV to 850 mV. On the other hand, the CO and HC samples experienced only a slight increase in OCV when they were inserted as powders, with the HC-P that achieved the highest voltage (980 mV). The little effect of morphology on these two samples could be advantageous for their use at the industrial scale, as the milling and sieving steps would not be necessary, thus avoiding the generation and dispersion of particulate matter into the environment, which can be a problem from a human health perspective [91–93].

3.2.2. Linear Scan Voltammetry

Fig. 5 shows the voltage vs. current density (*V-i*) and power vs. current density (*P-i*) curves at 450 °C obtained from the LSV tests, whereas the main electrical parameters (I_{lim}: limiting current density, *R:* system resistance, P_{max}: peak power density and I_{pmax}: current density at peak power) are summarized in (Table 4). Similar to what observed for the OCVs, the electrical values associated to the LSV test and, in particular, the peak power densities are comparable or slightly lower than the ones reported in other studies; however, it is possible to attribute the lower performance to the lower working temperature, fuels and

Table 4
Electrical performance of the fuel cell (I_{lim}: limiting current density, R: system resistance, P_{max}: peak power density, I_{pmax}: current density at peak power, GR: electrographite, CO: coke, BC: biochar, HC: hydrochar, C: bulk/pelletized morphology, P: powder morphology).

Sample		I_{lim} [mA/cm^2]	P_{max} [mW/cm^2]	I_{pmax} [mA/cm^2]	R [Ωcm^2]
GR	**C**	*23*	*0.9*	*13*	–
	P	*90*	*18.7*	*50*	*6.51*
CO	**C**	*70*	*15.4*	*33*	*10.79*
	P	*190*	*49.6*	*103*	*4.49*
BC	**C**	*121*	*14.9*	*76*	*3.54*
	P	*77*	*23.5*	*46*	*7.62 (14.17[a])*
HC	**C**	*76*	*15.8*	*47*	*12.22*
	P	*63*	*18.2*	*35*	*14.73*

[a] Value during the mass flow control.

the wide range of optimization of the cell design used in this work [32,50,70,85–87,94–97].

Although, in general, most of the *V-i* curves can be assumed to be linear, meaning that the polarization occurs in ohmic resistance control with the slope of the curve equal to the internal resistance of the system, the GR-C and BC-P samples (Fig. 5a,e) were characterized by different behavior. Specifically, the former was characterized by a significant instantaneous voltage drop due to the presence of activation losses, while the latter was characterized by the occurrence of mass transfer. Since activation losses are strongly correlated with the electrochemical reaction occurring on the fuel surface, it is possible to assume that the presence of pitch and the smoothness of the GR-C sample surface acted as an inhibitor, increasing the energy barrier required to initiate the carbon oxidation reaction [98]. To overcome this issue, it would be possible to modify the surface morphology by increasing its roughness, and consequently the S/V ratio, through machining or increase in the working temperature of the cell, since the activation energy is inversely proportional to it. Indeed, the GR-P sample was characterized by a polarization curve under ohmic resistance control and a peak power comparable to (or even larger than) other DCFC operating at higher temperature and with pure graphite [86,99,100].

Even though the peak power density of the CO-C sample was comparable with that of the BC-C and HC-C (~15 mW/cm^2), the powder morphology obtained surprisingly higher results if compared to the

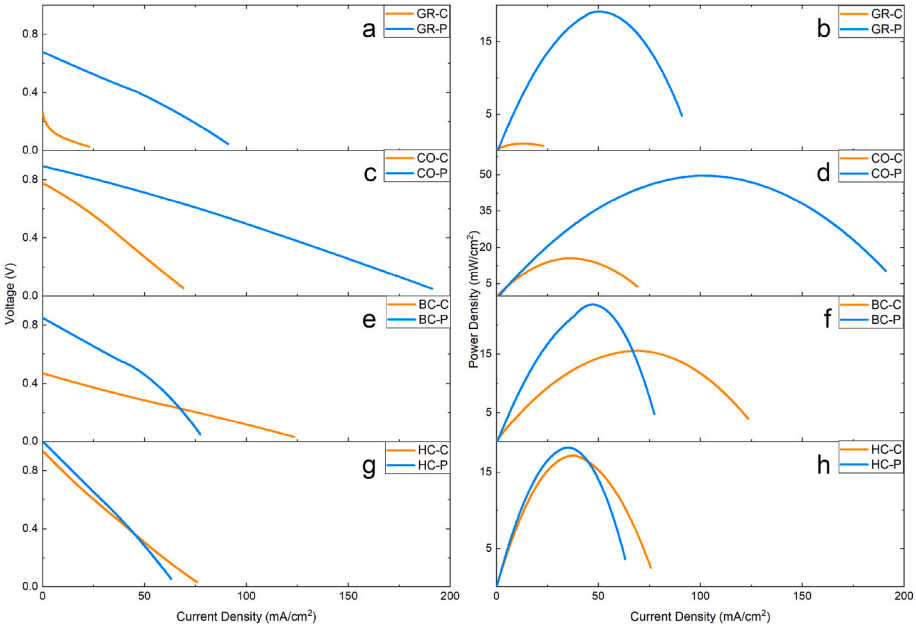

Fig. 5. Voltage vs. current density (V-i) and power vs. current density (P-i) polarization curves of the fuels ((a,b) GR: electrographite, (c,d) CO: coke, (e,f) BC: biochar, (g,h) HC: hydrochar, C: bulk/pelletized morphology, P: powder morphology).

other fuels (49.6 mW/cm^2) probably due to its property (chemical composition, degree of graphitization and S/V ratio) as previously discussed. Furthermore, the resistance of the system decreased from 10.79 Ωcm^2 to 4.49 Ωcm^2 once that the CO was inserted as powder.

Similarly, the BC-P peak power increased 1.5 times respect to the respective bulk morphology sample (23.5 vs. 14.9 mW/cm^2) thanks to the enhanced reactivity of the fuel given by the higher S/V ratio. However, the higher power density should be attributed to the higher starting OCV of the BC-P sample, since its *V-i* curve (Fig. 5e) was characterized by a higher slope, respect to the BC-C curve (Fig. 5e), and consequently higher resistance (3.54 Ωcm^2 vs. 7.62 Ωcm^2). However, because of the transition from ohmic resistance control to mass flow control, at about 60 mA/cm^2, the overall resistance almost doubled to 14.17 Ωcm^2, which limited the final value of current density to ~75 mA/cm^2. In addition, it can be hypothesized that the change in slope of the BC-P sample *V-i* curve (Fig. 5e) could also be due to the seep of some powder between the metal mesh of the anode, which polluted the electrolyte by carbonation (Eq. (4)), inhibiting the oxidation reaction [32].

$$C + 6OH^- = CO_3^{2-} + 3H_2O + 4e^- \quad (4)$$

On the other hand, the HC samples were characterized by a peculiar behavior with the *V-i* and *P-i* curves (Fig. 5g and h) almost perfectly overlapping, with peak power densities and resistances of 15.8 and 18.2 mW/cm^2 and 12.22 and 14.73 Ωcm^2 for the HC-C and HC-P samples, respectively. It is possible to assume that the binder used for agglomeration disaggregates upon contact with the hot electrolyte, resulting in a subsequent change in morphology from bulk/pellet to powder/sand. Contrary to BC-P sample, no mass flow control transition was observed at higher current densities, whereas the comparable performance of HC-C and HC-P samples strengthens the hypothesis of its direct introduction as a pellet rather than a powder. Finally, by observing the maximum power densities of the HC sample, it is possible to speculate that although it is characterized by the lowest fixed carbon, the presence of catalytic phases within the ash may have played an important role during the electrical characterization [49,80,81].

3.2.3. Galvanostatic analysis

The voltage-time (*V-t*) curves and their main characteristic values obtained at 450 °C and with an imposed current density equal to the fuel specific I_{pmax} are presented in Fig. 6 and Table 5, respectively. Given the high activation energy and low electrical performance, only GR-P was tested for electrographite.

In general, all fuels reached the steady state voltage (*SSV*) in less than 50 s, with only the CO-C and HC-P samples that required a longer time to achieve a constant voltage. Furthermore, their voltage drops (ΔV_g), defined as the difference between the starting voltage and the SSV, appeared smoother, as evidenced by the higher time constant (τ), and more prolonged in time than the other samples. Fuel morphology seems to strongly influence both the starting and SSV; indeed, when inserted as powder the CO, BC and HC samples increased their SSV of two, four and three times, respectively. In particular, BC-P achieved the best galvanostatic performances overall, with the highest starting voltage and SSV, the smallest ΔV_g and the second smallest characteristic time. It can be assumed that the higher S/V ratio provided by the powder and the presence of catalysts have greatly improved the performance. Furthermore, since the imposed current is less than 60 mA/cm^2, the BC-P behavior can be described as under ohmic control.

Finally, voltage drop appears to be unaffected by morphology, having comparable values among the same fuel type. Similarly, no correlation was observed between *V-t* and system resistance.

Table 5
Fuels performance at 450 °C and an imposed current density equal to I_{pmax} (τ: curve time constant, GR: electrographite, CO: coke, BC: biochar, HC: hydrochar, C: bulk/pelletized morphology, P: powder morphology).

	GR		CO		BC		HC	
	C	P	C	P	C	P	C	P
τ [s]	–	*12*	*21*	*15*	*5*	*8*	*8*	*26*
Steady state time [s]	–	*49*	*76*	*33*	*25*	*40*	*91*	*50*
Steady state voltage [mV]	–	*358*	*181*	*364*	*119*	*498*	*88*	*249*
Voltage drop [mV]	–	*153*	*315*	*315*	*187*	*147*	*273*	*288*

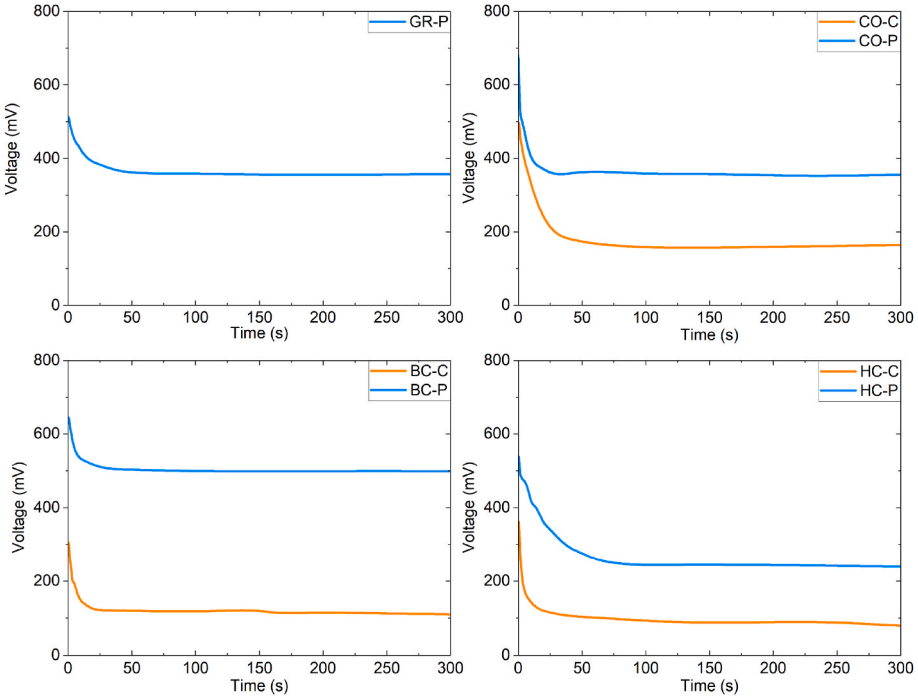

Fig. 6. Voltage vs. time (V−t) galvanostatic curves of the fuels at 450 °C and an imposed current density equal to I_{pmax} (GR: electrographite, CO: coke, BC: biochar, HC: hydrochar, C: bulk/pelletized morphology, P: powder morphology).

In Fig. 7 and Table 5 are presented the voltage vs. time (*V-t*) curves and their main characteristic values obtained at 450 °C and 100 mA divided per fuel morphology.

Similar to what was observed for the *V-t* curves at I_{pmax}, all three coarse morphology fuels reached SSVs in less than 90 s, which is perfectly in line with what Guo et al. observed from galvanostatic measurements at 450 °C and 100 mA in a NaOH/KOH eutectic mixture [32]. Overall, the BC-C sample achieved the highest SSV, the lowest time constant and the lowest voltage drop.

Except for the BC-P sample, the use the CO-P and HC-P samples led to an overall improvement of both the initial and SSVs, with the former showing the best overall electrical performance. It is noteworthy that, although the parameters of the HC-P sample were improved, its voltage continued to decrease over time, with a smooth transient time that did not allow to evaluate the sample time constant.

It has to be highlighted that also the BC-P *V-t* curve did not reach a steady value during the test time, although the steeper drop during the first tens of seconds allowed the time constant to be evaluated. In addition, its significant ΔV_g, the highest observed among all *V-t* curves, severely penalized its performance. Therefore, it is possible to assume that, because the test was carried out at a current density close to 60 mA/cm^2, the BC-P sample was within the mass flow control regime, which could have hindered its electrical properties.

Finally, trying to relate the system resistances obtained during the LSV analysis to the SSV, corresponding time and voltage drop, an inverse relationship was observed for the latter two parameters and a direct relationship with the former, although further analysis should be conducted to validate this hypothesis.

3.3. Steel mesh anode characterization

At the end of each test, morphological and chemical analysis by XRD and Scanning Electron Microscopy (SEM) of the AISI 304 mesh, used as the anode in the fuel cell, was performed to reveal the presence of corrosion products or pollutants on its surface.

In particular, corrosion of the mesh can have two undesirable consequences: on one hand, it decreases the effective exchange area, or even plugs the mesh itself, preventing an optimal contact between the solid fuel and the molten electrolyte, which is necessary to maintain a constant oxidation rate; on the other hand, due to the lower electrical conductivity, the electron transfer rate would also be reduced. The XRD spectra and SEM micrograph of the steel mesh before and after the electrochemical tests, are presented in Figs. 8 and 9, respectively.

XRD spectra of the steel mesh showed only the presence of ferrite (44.18°, 64.25°, 81.28° and 97.54°) and austenite (43°, 50°, 73.56° and 89.18°) with no trace of trona ($Na_3(CO_3)(HCO_3 \cdot 2H_2O)$ or thermonatrite ($Na_2(CO_3) \cdot H_2O$), which are common indicators of electrolyte carbonation [69].

In contrast, morphological alteration of the mesh surface was observed in SEM micrographs by local Energy-Dispersive X-Ray Spectroscopy (EDS). The spectra, reported in Table 6, identified the presence of only C, Cr and Fe on the mesh surface prior to its use, as expected from the AISI 304 chemical composition, along with the presence of small carbon particulate, attributable to some dust deposited on the sample surface (Spectra 1 and 2) (see Table 7).

The mesh surface appearance was severely modified after the electrochemical analysis. The generation of Na and K compounds was observed, which can be traced back to the recrystallization of the molten electrolyte (Spectra 3 and 4). Furthermore, the increase of Cr oxide compounds on the surface can be assumed (Spectrum 3), as also observed in other works in which the final amount of Cr_2O_3 increased after the immersion of the AISI 304 in an alkaline environment [68].

Finally, although some small carbon particles remained trapped in the crossing part of the mesh, no significant reduction in the potential exchange area was observed (Spectrum 5).

3.4. Applicability survey

To contextualize the application of MH-DCFCs to EAF steelshops, either alone or in addition to other possible power generation technologies already applicable in steel mills and based primarily on the waste heat-to-power concept, it is necessary to assess, as a first step, primarily the burden such a transition would have on available biomass, taking into account the increasing presence on site as alternative carbon sources. Therefore, for simplicity and ease of data retrieval, this preliminary mass balance will be based in the Italian context. In Italy, steel production from EAF in 2021 reached 20.4 Mton, accounting for more than 80% of total national production, with an electricity demand of at least 350 kWh per ton of liquid steel [6]. Assuming an increase in EAF share to cover the entire domestic steel production (24 Mton), the energy would be 8400 kWh/y (960 MW). Considering that about 0.5 g of fuel per cm^2 was placed in the anode configuration used in this work, and assuming a power density equal to that of the HC-P sample (15.8 mW/cm^2), a stack efficiency of 0.8 and a cell efficiency of 0.6, and the conservative goal of supplying at least 10% of the EAF annual electricity demand, this yields a total of about 6.3 kton of hydrochar per year, which could easily be covered by current annual biomass production in Italy, without burdening its request by the EAF cycle [30,33,34,51].

Consequently, the application of MH-DCFC technology fueled by biomass-derived materials, particularly hydrochar, seems a profitable new way to increase the overall efficiency of EAF. This is because, compared with other biomass related energy production technologies (e.g., co-firing, dedicated steam cycles, gasification) the conversion efficiency of MH-DCFCs would be higher, especially if coupled with other technologies already implemented, such as ORC [55,61,62]. For example, Salimbeni et al. [63] highlighted that only one-third of the heat recoverable from EAF flue gases is sufficient to cover the energy needs for heating a pyrolysis pilot plant operating at 550 °C. Hence,

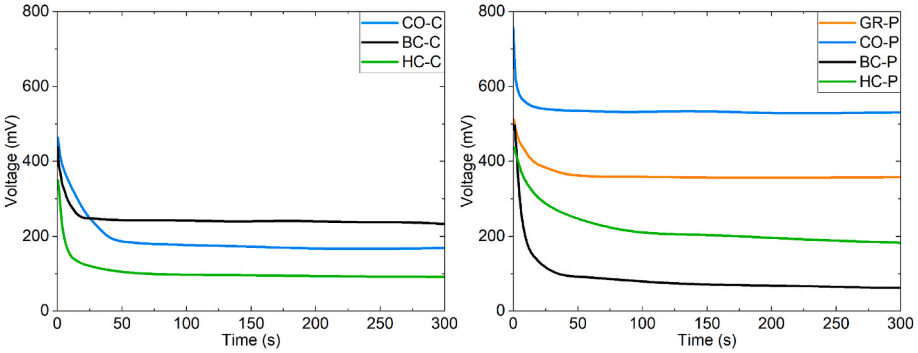

Fig. 7. Voltage vs. time (V−t) galvanostatic curves of the fuels at 450 °C and an imposed current equal to 100 mA (GR: electrographite, CO: coke, BC: biochar, HC: hydrochar, C: bulk/pelletized morphology, P: powder morphology).

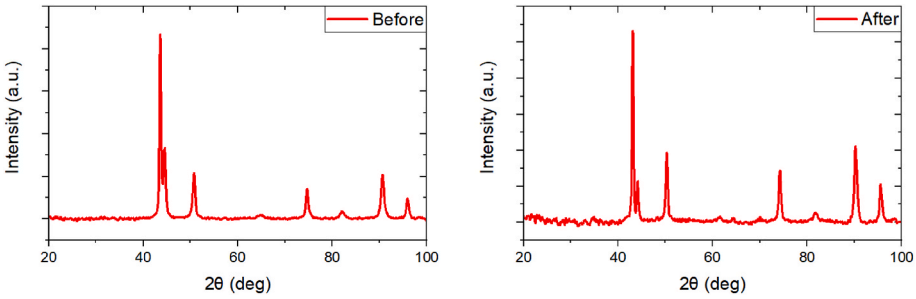

Fig. 8. XRD spectra of the AISI 304 mesh before and after the electrochemical test.

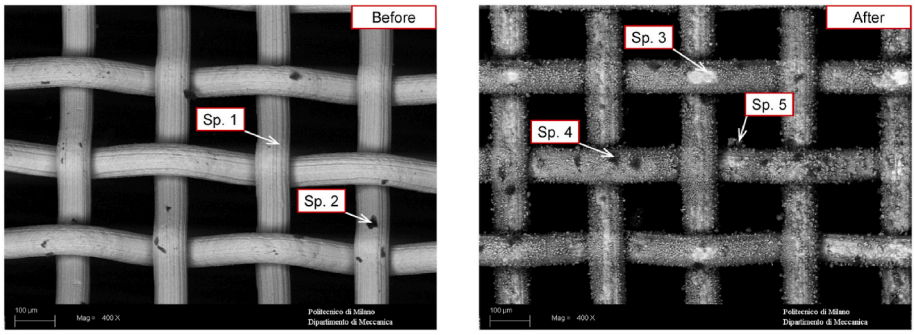

Fig. 9. SEM-BSE micrographs of the AISI 304 mesh before and after the electrochemical test.

Table 6
Fuels performance at 450 °C and an imposed current density equal to 100 mA (τ: curve time constant, GR: electrographite, CO: coke, BC: biochar, HC: hydrochar, C: bulk/pelletized morphology, P: powder morphology).

	GR		CO		BC		HC	
	C	P	C	P	C	P	C	P
Tau [s]	–	*12*	*20*	*5*	*6*	*16*[a]	*8*	*13*[a]
Steady state time [s]	–	*51*	*51*	*45*	*25*	–	*87*	–
Steady state voltage [mV]	–	*354*	*180*	*533*	*245*	*200*[a]	*93*	*75*[a]
Voltage drop [mV]	–	*157*	*283*	*224*	*192*	*417*[a]	*255*	*226*[a]

[a] Evaluated at 100 s.

Table 7
EDS spectra of the AISI 304 (spectra referred to Fig. 9).

Spectrum	Mesh Condition	C [% wt.]	O [% wt.]	Na [% wt.]	K [% wt.]	Cr [% wt.]	Fe [% wt.]
1	*Before*	*12.33*	–	–		*17.2*	*64.02*
2	*Before*	*100.00*	–	–	–	–	–
3	*After*	*5.85*	*18.73*	*3.90*	–	*7.74*	*64.02*
4	*After*	*45.21*	*17.99*	*5.79*	*3.81*	–	*15.49*
5	*After*	*100.00*	–	–	–	–	–

there should be a sufficient amount of waste heat that can be exploited for heating the fuel cell. As a final thought, although coke appeared to be the most efficient fuel, its use could easily be avoided, along with the emissions associated with its production, while the use of pulverized electrographite could still be beneficial, especially when loaded together with hydrochar or biochar as fuel.

4. Conclusions

The feasibility of four carbon materials related to steelmaking processes, particularly to the scrap recycling route, as fuels in an MH-DCFC was investigated. OCV, LSV and galvanostatic measurements were carried out to evaluate the performance of the fuels introduced in two different morphologies, namely coarse/pellet and powder (granulometry: 125–500 μm). Finally, physical and chemical characterization of the fuels was performed to better understand their electrical behavior and performance, which can be summarized as follows:

1. The introduction of powder fuels has led to an overall increase in maximum power density.
2. Coke provided the highest electrical performance as both coarse and powder fuel (15.4 vs. 49.6 mW/cm^2, respectively).
3. Electrographite, although having a high fixed carbon content (85.20 wt%), was only applicable in powder morphology (18.7 mW/cm^2) because of the strong inhibitory effect of pitch when inserted as a coarse fuel (0.9 mW/cm^2).
4. Biochar and hydrochar were characterized by lower penalties in terms of electrical performance when introduced as pellets (14.9 vs. 23.5 mW/cm^2 and 15.8 vs. 18.2 mW/cm^2, respectively).
5. Although hydrochar is characterized by the lowest fixed carbon content among all fuels (0.66 %wt.), the presence of catalytic phases in its ash (hematite and periclase), may have played an important role in its electrical behavior, achieving maximum power densities comparable to those of powdered electrographite and biochar.

Funding

This research was supported by the Italian Ministry for Education, University and Research (MIUR) through the "Department of Excellence LIS4.0" project (Integrated Laboratory for Lightweight and Smart Structures).

Conflict of interest declaration

On behalf of all authors, the corresponding author states that there is no conflict of interest.

Authors statement

Gianluca Dall'Osto: conceptualization, methodology, visualization, editing, writing - original draft. Davide Mombelli: data curation, resources, writing - original draft. Andrea Pittalis: formal analysis, investigation, data curation, writing – original draft. Carlo Mapelli: supervision.

Declaration of competing interest

The authors declare that they have no known competing financial interests or personal relationships that could have appeared to influence the work reported in this paper.

Data availability

The data that has been used is confidential.

Acknowledgements

The Authors would like to acknowledge Dr. Marco Alloni (Prosimet S.p.A. – Filago (BG), Italy) for TG-DSC analysis.

List of symbols

A	Ash
BC	Pelletized Biochar
BF	Blast Furnace
C	Bulk Granule/Pelletized Morphology
CCS	Carbon Capture and Storage
CE	Counter Electrode
CO	Coke
DCFC	Direct Carbon Fuel Cell
EAF	Electric Arc Furnace
EDS	Energy-Dispersive X-Ray Spectroscopy
FC	Fixed Carbon
GR	Electrographite
HC	Pelletized Hydrochar
I_{lim}	Limiting Current Density
I_{pmax}	Current Density at Peak Power
LSV	Linear Scan Voltammetry
M	Moisture
MCFC	Molten Carbonate Fuel Cell
MH-DCFC	Molten Hydroxide DCFC
OCV	Open Cell Voltage
P	Powder Morphology
P_{max}	Peak Power Density
R	System Resistance
S/V	Surface-To-Volume Ratio
SEM	Scanning Electron Microscopy
SSV	Steady State Voltage
TG-DSC	Thermogravimetric and Differential Scanning Calorimetry
V	Voltage
VM	Volatile Matter
WE	Working Electrode
XRD	X-Ray Diffraction
ΔV_g	Voltage Drop
τ	Time Constant

References

[1] A. Di Schino, Environmental impact of steel industry, in: Handbook of Environmental Materials Management, Springer International Publishing, Cham, 2018, pp. 1–21, https://doi.org/10.1007/978-3-319-58538-3_101-1.
[2] International Energy Agency, Iron and Steel Analysis, 2022. https://www.iea.org/reports/iron-and-steel. (Accessed 5 November 2022).
[3] H. Mandova, P. Patrizio, S. Leduc, J. Kjärstad, C. Wang, E. Wetterlund, F. Kraxner, W. Gale, Achieving carbon-neutral iron and steelmaking in Europe through the deployment of bioenergy with carbon capture and storage, J. Clean. Prod. 218 (2019) 118–129, https://doi.org/10.1016/j.jclepro.2019.01.247.
[4] T. Echterhof, Review on the use of alternative carbon sources in EAF steelmaking, Metals 11 (2021) 222, https://doi.org/10.3390/met11020222.
[5] C. Bataille, M. Åhman, K. Neuhoff, L.J. Nilsson, M. Fischedick, S. Lechtenböhmer, B. Solano-Rodriquez, A. Denis-Ryan, S. Stiebert, H. Waisman, O. Sartor, S. Rahbar, A review of technology and policy deep decarbonization pathway options for making energy-intensive industry production consistent with the Paris Agreement, J. Clean. Prod. 187 (2018) 960–973, https://doi.org/10.1016/J.JCLEPRO.2018.03.107.
[6] C. Mapelli, G. Dall'Osto, D. Mombelli, S. Barella, A. Gruttadauria, Future scenarios for reducing emissions and consumption in the Italian steelmaking industry, Steel Res. Int. 93 (2022), 2100631, https://doi.org/10.1002/srin.202100631.
[7] C.M. Nwachukwu, E. Olofsson, R. Lundmark, E. Wetterlund, Evaluating fuel switching options in the Swedish iron and steel industry under increased competition for forest biomass, Appl. Energy 324 (2022), 119878, https://doi.org/10.1016/j.apenergy.2022.119878.
[8] H. Mandova, S. Leduc, C. Wang, E. Wetterlund, P. Patrizio, W. Gale, F. Kraxner, Possibilities for CO2 emission reduction using biomass in European integrated steel plants, Biomass Bioenergy 115 (2018) 231–243, https://doi.org/10.1016/j.biombioe.2018.04.021.
[9] International Energy Agency, Iron and Steel Technology Roadmap towards More Sustainable Steelmaking Part of the Energy Technology Perspectives Series, 2020. https://www.iea.org/reports/iron-and-steel-technology-roadmap. (Accessed 5 November 2022).
[10] D. Mombelli, G. Dall'Osto, C. Mapelli, A. Gruttadauria, S. Barella, Modeling of a continuous charging electric Arc Furnace metallic loss based on the charge mix, Steel Res. Int. 92 (2021), 2000580, https://doi.org/10.1002/srin.202000580.
[11] Biochar for a Sustainable EAF Steel Production, GREENEAF2) - Publications Office of the EU, 2018. https://op.europa.eu/en/publication-detail/-/publication/7198c147-22b2-11e9-8d04-01aa75ed71a1/language-en. (Accessed 6 July 2023).
[12] Sustainable EAF Steel Production, GREENEAF) - Publications Office of the EU, 2013. https://op.europa.eu/en/publication-detail/-/publication/e7dc500c-82de-4c2d-8558-5e24a2d335fb/language-en. (Accessed 6 July 2023).
[13] T. Meier, T. Hay, T. Echterhof, H. Pfeifer, T. Rekersdrees, L. Schlinge, S. Elsabagh, H. Schliephake, Process modeling and simulation of biochar usage in an electric Arc Furnace as a substitute for fossil coal, Steel Res. Int. 88 (2017), 1600458, https://doi.org/10.1002/srin.201600458.
[14] X.-M. He, S. Yi, P.-R. Fu, X.-C. Zeng, D. Zhang, X.-H. Cheng, Combustion reactivity of biochar and char generated from Co-pyrolysis of coal and four additives: application in blast furnace, J. Energy Eng. 143 (2017), https://doi.org/10.1061/(ASCE)EY.1943-7897.0000369.
[15] R. Robinson, L. Brabie, M. Pettersson, M. Amovic, R. Ljunggren, An empirical comparative study of renewable biochar and fossil carbon as carburizer in steelmaking, ISIJ Int. 62 (2022), https://doi.org/10.2355/isijinternational.ISIJINT-2020-135. ISIJINT-2020-135.
[16] A. Cardarelli, M. De Santis, F. Cirilli, M. Barbanera, Computational fluid dynamics analysis of biochar combustion in a simulated ironmaking electric arc furnace, Fuel 328 (2022), 125267, https://doi.org/10.1016/j.fuel.2022.125267.
[17] C. DiGiovanni, D. Li, K.W. Ng, X. Huang, Ranking of injection biochar for slag foaming applications in steelmaking, Metals 13 (2023) 1003, https://doi.org/10.3390/met13061003.
[18] Y. Lu, H. Yang, A.V. Karasev, C. Wang, P.G. Jönsson, Applications of hydrochar and charcoal in the iron and steelmaking industry—Part 1: characterization of carbonaceous materials, Sustainability 14 (2022) 9488, https://doi.org/10.3390/su14159488.
[19] C. Zhang, G. Wang, X. Ning, J. Zhang, C. Wang, Numerical simulation of combustion behaviors of hydrochar derived from low-rank coal in the raceway of blast furnace, Fuel 278 (2020), 118267, https://doi.org/10.1016/j.fuel.2020.118267.
[20] G. Wang, J. Zhang, J.-Y. Lee, X. Mao, L. Ye, W. Xu, X. Ning, N. Zhang, H. Teng, C. Wang, Hydrothermal carbonization of maize straw for hydrochar production and its injection for blast furnace, Appl. Energy 266 (2020), 114818, https://doi.org/10.1016/j.apenergy.2020.114818.
[21] L. Ye, J. Zhang, G. Wang, C. Wang, X. Mao, X. Ning, N. Zhang, H. Teng, J. Li, C. Wang, Feasibility analysis of plastic and biomass hydrochar for blast furnace injection, Energy 263 (2023), 125903, https://doi.org/10.1016/j.energy.2022.125903.
[22] T. Norgate, D. Langberg, Environmental and economic aspects of charcoal use in steelmaking, ISIJ Int. 49 (2009) 587–595, https://doi.org/10.2355/isijinternational.49.587.
[23] T. Norgate, N. Haque, M. Somerville, S. Jahanshahi, Biomass as a source of renewable carbon for iron and steelmaking, ISIJ Int. 52 (2012) 1472–1481, https://doi.org/10.2355/isijinternational.52.1472.
[24] T. Demus, T. Reichel, T. Echterhof, H. Pfeifer, Biochar usage in EAF-steelmaking potential and feasibility, in: Proceedings of the 1st European Steel Technology \& Application Days (ESTAD) \& 31st Journées Sidérurgiques Internationales (JSI), 2014, pp. 7–8. Paris, France.
[25] International Energy Agency, Electricity, 2022. https://www.iea.org/fuels-and-technologies/electricity. (Accessed 23 September 2022).
[26] L. Mastropasqua, L. Pierangelo, M. Spinelli, M.C. Romano, S. Campanari, S. Consonni, Molten Carbonate Fuel Cells retrofits for CO2 capture and enhanced

energy production in the steel industry, Int. J. Greenh. Gas Control 88 (2019) 195–208, https://doi.org/10.1016/j.ijggc.2019.05.033.
[27] L. Mastropasqua, L. Pierangelo, M. Spinelli, M.C. Romano, S. Campanari, S. Consonni, Molten Carbonate Electrochemical Membranes for Low-Carbon Retrofits in the Steel Industry, 2018.
[28] M. Spinelli, S. Campanari, S. Consonni, M.C. Romano, T. Kreutz, H. Ghezel-Ayagh, S. Jolly, Molten carbonate fuel cells for retrofitting postcombustion CO2 capture in coal and natural gas power plants, Journal of Electrochemical Energy Conversion and Storage (2018) 15, https://doi.org/10.1115/1.4038601.
[29] M. Spinelli, M.C. Romano, S. Consonni, S. Campanari, M. Marchi, G. Cinti, Application of molten carbonate fuel cells in cement plants for CO2 capture and clean power generation, Energy Proc. 63 (2014) 6517–6526, https://doi.org/10.1016/j.egypro.2014.11.687.
[30] S. Giddey, S.P.S. Badwal, A. Kulkarni, C. Munnings, A comprehensive review of direct carbon fuel cell technology, Prog. Energy Combust. Sci. 38 (2012) 360–399, https://doi.org/10.1016/j.pecs.2012.01.003.
[31] H. Watanabe, T. Shimada, M. Nakanouchi, K. Hanamura, Impact of mass transfer in the carbon/carbonate-packed bed on the power output of a press-type direct carbon fuel cell, Energy Fuels 33 (2019) 12865–12870, https://doi.org/10.1021/acs.energyfuels.9b03032.
[32] L. Guo, J.M. Calo, E. DiCocco, E.J. Bain, Development of a low temperature, molten hydroxide direct carbon fuel cell, Energy Fuels 27 (2013) 1712–1719, https://doi.org/10.1021/ef302100h.
[33] A. Kacprzak, R. Kobyłecki, R. Włodarczyk, Z. Bis, Efficiency of non-optimized direct carbon fuel cell with molten alkaline electrolyte fueled by carbonized biomass, J. Power Sources 321 (2016) 233–240, https://doi.org/10.1016/J.JPOWSOUR.2016.04.132.
[34] V. Hoffmann, D. Jung, J. Zimmermann, C. Rodriguez Correa, A. Elleuch, K. Halouani, A. Kruse, Conductive carbon materials from the hydrothermal carbonization of vineyard residues for the application in electrochemical double-layer capacitors (EDLCs) and direct carbon fuel cells (DCFCs), Materials 12 (2019) 1703, https://doi.org/10.3390/ma12101703.
[35] Graphite Electrode Price - Updating - DanCrabon, 2022. https://www.dancarbon.com/q/graphite-electrode/84.html. (Accessed 17 October 2022).
[36] G. Wei, R. Zhu, S. Yang, S. Hu, L. Yang, F. Chen, Carbon powder mixed injection with a shrouding supersonic oxygen jet in electric Arc Furnace steelmaking, Metall. Mater. Trans. B 51 (2020) 2298–2308, https://doi.org/10.1007/s11663-020-01920-x.
[37] M. Zaharia, V. Sahajwalla, N. Saha-Chaudhury, P. O'kane, A. Fontana, C. Skidmore, D. Knights, Recycling of rubber tyres in electric Arc Furnace steelmaking: carbon/slag reactions of coke/rubber blends, High Temp. Mater. Process. 31 (2012) 593–602, https://doi.org/10.1515/htmp-2012-0096.
[38] V. Sahajwalla, M. Rahman, R. Khanna, N. Saha-Chaudhury, P. O'Kane, C. Skidmore, D. Knights, Recycling waste plastics in EAF steelmaking: carbon/slag interactions of HDPE-coke blends, Steel Res. Int. 80 (2009) 535–543, https://doi.org/10.2374/SRI08SP168.
[39] V. Mambakkam, R. Alicandri, K. Chattopadhyay, SPL as a carbon injection source in an EAF: a process study, in: C. Chesonis (Ed.), Light Metals 2019, Springer International Publishing, Cham, 2019, pp. 857–866.
[40] M. Rd, H. Rodriguez-Hernández, C. An, A mathematical simulator for the EAF steelmaking process using direct reduced iron, ISIJ Int. 41 (2001) 426–436.
[41] A.-G. Guézennec, J.-C. Huber, F. Patisson, P. Sessiecq, J.-P. Birat, D. Ablitzer, Dust formation in electric Arc Furnace: birth of the particles, Powder Technol. 157 (2005) 2–11, https://doi.org/10.1016/j.powtec.2005.05.006.
[42] J. Jezierski, K. Janerka, Pneumatic powder injection technique as a tool for waste utilization, Int. J. Environ. Waste Manag. 2 (2008) 636–646.
[43] X. Zhou, V. Strezov, Y. Jiang, X. Yang, J. He, T. Evans, Life cycle impact assessment of airborne metal pollution near selected iron and steelmaking industrial areas in China, Aerosol Air Qual. Res. (2019), https://doi.org/10.4209/aaqr.2019.10.0552.
[44] J. Madias, Electric furnace steelmaking, in: Treatise on Process Metallurgy, 2014, pp. 271–300, https://doi.org/10.1016/B978-0-08-096988-6.00013-4. Elsevier.
[45] R. Cappelletti, M. Ceppi, J. Claudatus, V. Gennaro, Health status of male steel workers at an electric arc furnace (EAF) in Trentino, Italy, J. Occup. Med. Toxicol. 11 (2016) 7, https://doi.org/10.1186/s12995-016-0095-8.
[46] C. Li, H. Yi, D. Lee, On-demand supply of slurry fuels to a porous anode of a direct carbon fuel cell: attempts to increase fuel-anode contact and realize long-term operation, J. Power Sources 309 (2016) 99–107, https://doi.org/10.1016/j.jpowsour.2016.01.080.
[47] A. Ali, F. Shehzad Bashir, R. Raza, A. Rafique, M. Kaleem Ullah, F. Alvi, M. Afzal, M. Ghauri, L.M. Belova, Electrochemical study of composite materials for coal-based direct carbon fuel cell, Int. J. Hydrogen Energy 43 (2018) 12900–12908, https://doi.org/10.1016/j.ijhydene.2018.05.104.
[48] W. Hao, X. He, Y. Mi, Achieving high performance in intermediate temperature direct carbon fuel cells with renewable carbon as a fuel source, Appl. Energy 135 (2014) 174–181, https://doi.org/10.1016/j.apenergy.2014.08.055.
[49] A. Elleuch, K. Halouani, Y. Li, Investigation of chemical and electrochemical reactions mechanisms in a direct carbon fuel cell using olive wood charcoal as sustainable fuel, J. Power Sources 281 (2015) 350–361, https://doi.org/10.1016/j.jpowsour.2015.01.171.
[50] S. Eom, J. Cho, S. Ahn, Y. Sung, G. Choi, D. Kim, Comparison of the electrochemical reaction parameter of graphite and sub-bituminous coal in a direct carbon fuel cell, Energy Fuels 30 (2016) 3502–3508, https://doi.org/10.1021/acs.energyfuels.5b02904.
[51] ISPRA, Rapporto Rifiuti Urbani 2021, 2022. https://www.isprambiente.gov.it/it/pubblicazioni/rapporti/rapporto-rifiuti-urbani-edizione-2022. (Accessed 7 November 2022).
[52] M. Escala, T. Zumbühl, Ch Koller, R. Junge, R. Krebs, Hydrothermal carbonization as an energy-efficient alternative to established drying technologies for sewage sludge: a feasibility study on a laboratory scale, Energy Fuels 27 (2013) 454–460, https://doi.org/10.1021/ef3015266.
[53] S.K. Hoekman, A. Broch, C. Robbins, Hydrothermal carbonization (HTC) of lignocellulosic biomass, Energy Fuels 25 (2011) 1802–1810, https://doi.org/10.1021/ef101745n.
[54] K. Weber, S. Heuer, P. Quicker, T. Li, T. Løvås, V. Scherer, An alternative approach for the estimation of biochar yields, Energy Fuels 32 (2018) 9506–9512, https://doi.org/10.1021/acs.energyfuels.8b01825.
[55] S. Lecompte, O. Oyewunmi, C. Markides, M. Lazova, A. Kaya, M. van den Broek, M. De Paepe, Case study of an organic rankine cycle (ORC) for waste heat recovery from an electric Arc Furnace (EAF), Energies 10 (2017) 649, https://doi.org/10.3390/en10050649.
[56] Z. Zhang, L. Chen, B. Yang, Y. Ge, F. Sun, Thermodynamic analysis and optimization of an air Brayton cycle for recovering waste heat of blast furnace slag, Appl. Therm. Eng. 90 (2015) 742–748, https://doi.org/10.1016/j.applthermaleng.2015.07.057.
[57] W. Duan, Q. Yu, Z. Wang, J. Liu, Q. Qin, Life cycle and economic assessment of multi-stage blast furnace slag waste heat recovery system, Energy 142 (2018) 486–495, https://doi.org/10.1016/j.energy.2017.10.048.
[58] V. Colla, T.A. Branca, R. Pietruck, S. Wölfelschneider, A. Morillon, D. Algermissen, S. Rosendahl, H. Granbom, U. Martini, D. Snaet, Future research and developments on reuse and recycling of steelmaking by-products, Metals 13 (2023) 676, https://doi.org/10.3390/met13040676.
[59] H. Zhang, J. Dong, C. Wei, C. Cao, Z. Zhang, Future trend of terminal energy conservation in steelmaking plant: integration of molten slag heat recovery-combustible gas preparation from waste plastics and CO2 emission reduction, Energy 239 (2022), 122543, https://doi.org/10.1016/j.energy.2021.122543.
[60] C. Yue, D. Li, L. Li, Z. Xu, Development of waste heat recovery technology from steel slag, E3S Web of Conferences 385 (2023), 03001, https://doi.org/10.1051/e3sconf/202338503001.
[61] R. Pili, L. García Martínez, C. Wieland, H. Spliethoff, Techno-economic potential of waste heat recovery from German energy-intensive industry with Organic Rankine Cycle technology, Renew. Sustain. Energy Rev. 134 (2020), 110324, https://doi.org/10.1016/j.rser.2020.110324.
[62] T. Bause, F. Campana, L. Filippini, A. Foresti, N. Monti, T. Pelz, Cogeneration with ORC at elbe-stahlwerke feralpi EAF shop, AISTech - Iron and Steel Technology Conference Proceedings 1 (2014) 1101–1111.
[63] A. Salimbeni, G. Lombardi, A.M. Rizzo, D. Chiaramonti, Techno-Economic feasibility of integrating biomass slow pyrolysis in an EAF steelmaking site: a case study, Appl. Energy 339 (2023), 120991, https://doi.org/10.1016/j.apenergy.2023.120991.
[64] S. Zecevic, E.M. Patton, P. Parhami, Direct electrochemical power generation from carbon in fuel cells with molten hydroxide electrolyte, Chem. Eng. Commun. 192 (2005) 1655–1670, https://doi.org/10.1080/009864490896241.
[65] ASTM Standard, Standard Test Method for Chemical Analysis of Wood Charcoal, American Society for Testing and Materials, Conshohocken, PA, 2009.
[66] J.R. Crum, L.E. Shoemaker, Corrosion Resistance of Nickel Alloys in Caustic Solutions, 2006.
[67] J.B. Singh, Corrosion behavior of alloy 625, in: Alloy 625 : Microstructure, Properties and Performance, Springer Nature Singapore, Singapore, 2022, https://doi.org/10.1007/978-981-19-1562-8_7, 241–291.
[68] I. Hamidah, A. Solehudin, A. Setiawan, A. Hamdani, M.A.S. Hidayat, F. Adityawarman, F. Khoirunnisa, A.B.D. Nandiyanto, Corrosion study of AISI 304 on KOH, NaOH, and NaCl solution as an electrode on electrolysis process, J. Eng. Sci. Technol. 13 (2018) 1345–1351.
[69] B. Bozzini, S. Barella, F. Bogani, G. Giovannelli, S. Natali, G. Scarselli, M. Boniardi, Corrosion of Stainless Steel Grades in Molten NaOH/KOH Eutectic at 250 °C: AISI304 Austenitic and 2205 Duplex, Materials and Corrosion, 2012, https://doi.org/10.1002/maco.201106386 n/a-n/a.
[70] A. Kacprzak, R. Kobylecki, Z. Bis, Influence of temperature and composition of NaOH–KOH and NaOH–LiOH electrolytes on the performance of a direct carbon fuel cell, J. Power Sources 239 (2013) 409–414, https://doi.org/10.1016/j.jpowsour.2013.03.159.
[71] A.C. Lua, F.Y. Lau, J. Guo, Influence of pyrolysis conditions on pore development of oil-palm-shell activated carbons, J. Anal. Appl. Pyrolysis 76 (2006) 96–102, https://doi.org/10.1016/j.jaap.2005.08.001.
[72] S. Eom, S. Ahn, Y. Rhie, K. Kang, Y. Sung, C. Moon, G. Choi, D. Kim, Influence of devolatilized gases composition from raw coal fuel in the lab scale DCFC (direct carbon fuel cell) system, Energy 74 (2014) 734–740, https://doi.org/10.1016/j.energy.2014.07.039.
[73] H. Jang, J.D. Ocon, S. Lee, J.K. Lee, J. Lee, Direct power generation from waste coffee grounds in a biomass fuel cell, J. Power Sources 296 (2015) 433–439, https://doi.org/10.1016/j.jpowsour.2015.07.059.
[74] J. Mizusaki, H. Tagawa, K. Tsuneyoshi, A. Sawata, Reaction kinetics and microstructure of the solid oxide fuel cells air electrode La0.6Ca0.4MnO3/YSZ, J. Electrochem. Soc. 138 (1991) 1867–1873, https://doi.org/10.1149/1.2085891.
[75] N. Kaklidis, V. Kyriakou, I. Garagounis, A. Arenillas, J.A. Menéndez, G. E. Marnellos, M. Konsolakis, Effect of carbon type on the performance of a direct or hybrid carbon solid oxide fuel cell, RSC Adv. 4 (2014) 18792–18800, https://doi.org/10.1039/C4RA01022A.

[76] A.C. Chien, A. Arenillas, C. Jiang, J.T.S. Irvine, Performance of direct carbon fuel cells operated on coal and effect of operation mode, J. Electrochem. Soc. 161 (2014) F588–F593, https://doi.org/10.1149/2.025405jes.
[77] J. Yu, Y. Zhao, Y. Li, Utilization of corn cob biochar in a direct carbon fuel cell, J. Power Sources 270 (2014) 312–317, https://doi.org/10.1016/j.jpowsour.2014.07.125.
[78] A. Elleuch, A. Boussetta, J. Yu, K. Halouani, Y. Li, Experimental investigation of direct carbon fuel cell fueled by almond shell biochar: Part I. Physico-chemical characterization of the biochar fuel and cell performance examination, Int. J. Hydrogen Energy 38 (2013) 16590–16604, https://doi.org/10.1016/j.ijhydene.2013.08.090.
[79] X. Li, Z.H. Zhu, R. De Marco, A. Dicks, J. Bradley, S. Liu, G.Q. Lu, Factors that determine the performance of carbon fuels in the direct carbon fuel cell, Ind. Eng. Chem. Res. 47 (2008) 9670–9677, https://doi.org/10.1021/ie800891m.
[80] X. Li, Z. Zhu, R. De Marco, J. Bradley, A. Dicks, Evaluation of raw coals as fuels for direct carbon fuel cells, J. Power Sources 195 (2010) 4051–4058, https://doi.org/10.1016/j.jpowsour.2010.01.048.
[81] L.K. Palniandy, W.Y. Wong, J.J. Yap, V. Doshi, L.W. Yoon, Effect of alkaline pretreatment on rice husk-derived biochar for direct carbon fuel cell, J. Eng. Sci. Technol. (2017) 84–100.
[82] P. Engler, M.W. Santana, M.L. Mittleman, D. Balazs, Non-isothermal, in situ XRD analysis of dolomite decomposition, Thermochim. Acta 140 (1989) 67–76, https://doi.org/10.1016/0040-6031(89)87285-5.
[83] S. Gunasekaran, G. Anbalagan, Thermal decomposition of natural dolomite, Bull. Mater. Sci. 30 (2007) 339–344, https://doi.org/10.1007/S12034-007-0056-Z/METRICS.
[84] M. Olszak-Humienik, M. Jablonski, Thermal behavior of natural dolomite, J. Therm. Anal. Calorim. 119 (2015) 2239–2248, https://doi.org/10.1007/s10973-014-4301-6.
[85] A.C. Rady, S. Giddey, S.P.S. Badwal, B.P. Ladewig, S. Bhattacharya, Review of fuels for direct carbon fuel cells, Energy Fuels 26 (2012) 1471–1488, https://doi.org/10.1021/ef201694y.
[86] A. Kacprzak, R. Włodarczyk, Materials selection and construction development for ensuring the availability and durability of the molten hydroxide electrolyte direct carbon fuel cell (MH-MCFC), Materials 13 (2020) 4659, https://doi.org/10.3390/ma13204659.
[87] A. Kacprzak, R. Kobyłecki, R. Włodarczyk, Z. Bis, Efficiency of non-optimized direct carbon fuel cell with molten alkaline electrolyte fueled by carbonized biomass, J. Power Sources 321 (2016) 233–240, https://doi.org/10.1016/j.jpowsour.2016.04.132.
[88] Y. Li, H. Chen, A. Hammam, H. Wei, H. Nie, W. Ding, M. Omran, L. Yan, Y. Yu, Study of an organic binder of cold-bonded briquettes with two different iron bearing materials, Materials 14 (2021) 2952, https://doi.org/10.3390/ma14112952.
[89] S.-M. Lee, D.-S. Kang, J.-S. Roh, Bulk graphite: materials and manufacturing process, Carbon Letters 16 (2015) 135–146, https://doi.org/10.5714/CL.2015.16.3.135.
[90] D. Hulicova-Jurcakova, M. Kodama, S. Shiraishi, H. Hatori, Z.H. Zhu, G.Q. Lu, Nitrogen-enriched nonporous carbon electrodes with extraordinary supercapacitance, Adv. Funct. Mater. 19 (2009) 1800–1809, https://doi.org/10.1002/adfm.200801100.
[91] A. Očkajová, M. Kučerka, R. Kminiak, Ľ. Krišťák, R. Igaz, R. Réh, Occupational exposure to dust produced when milling thermally modified wood, Int. J. Environ. Res. Publ. Health 17 (2020) 1478, https://doi.org/10.3390/ijerph17051478.
[92] Y. Cheng, L. Liu, H. Wang, M. Wu, Y. Liu, Investigations on the dust distribution characteristics of dry milling using inserts with various groove profiles, Int. J. Adv. Des. Manuf. Technol. 74 (2014) 551–562, https://doi.org/10.1007/s00170-014-6019-9.
[93] T. Liu, S. Liu, The impacts of coal dust on miners' health: a review, Environ. Res. 190 (2020), 109849, https://doi.org/10.1016/j.envres.2020.109849.
[94] L. Xing, J. Hao, X. Li, Y. Zhang, Z. Hu, Y. Gao, Polarization modeling and performance optimization of a molten sodium hydroxide direct carbon fuel cell (MHDCFC), J. Power Sources 363 (2017) 428–441, https://doi.org/10.1016/j.jpowsour.2017.07.113.
[95] K. Bie, P. Fu, Y. Liu, A. Muhammad, Comparative study on the performance of different carbon fuels in a molten carbonate direct carbon fuel cell with a novel anode structure, J. Power Sources 460 (2020), 228101, https://doi.org/10.1016/j.jpowsour.2020.228101.
[96] K. Xu, J. Dong, X. Li, J. Wang, Z. Hu, A. Li, H. Yao, Evaluation of biomass and its thermal decomposition products as fuels for direct carbon fuel cells, Biomass Bioenergy 130 (2019), 105359, https://doi.org/10.1016/j.biombioe.2019.105359.
[97] W. Hao, P. Luo, Z. Wu, Y. Mi, Z. Gao, The effect of biomass pyrolysis temperature on the performance of biochar-fed molten hydroxide direct carbon fuel cells, Biomass Bioenergy 150 (2021), 106122, https://doi.org/10.1016/j.biombioe.2021.106122.
[98] J. Larminie, A. Dicks, M.S. McDonald, Fuel Cell Systems Explained, 2003. J. Wiley Chichester, UK.
[99] J.-P. Kim, H. Lim, C.-H. Jeon, Y.-J. Chang, K.-N. Koh, S.-M. Choi, J.-H. Song, Performance evaluation of tubular fuel cells fuelled by pulverized graphite, J. Power Sources 195 (2010) 7568–7573, https://doi.org/10.1016/j.jpowsour.2010.05.065.
[100] A. Elleuch, J. Yu, A. Boussetta, K. Halouani, Y. Li, Electrochemical oxidation of graphite in an intermediate temperature direct carbon fuel cell based on two-phases electrolyte, Int. J. Hydrogen Energy 38 (2013) 8514–8523, https://doi.org/10.1016/j.ijhydene.2012.11.070.